PROCEEDINGS OF SCIENCE

# International Linear Collider: Physics and Detectors

**Klaus Desch***
*Albert-Ludwigs-Universität Freiburg, Freiburg, Germany*
*E-mail:* desch@physik.uni-freiburg.de

The major physics motivation to construct the International Linear Collider (ILC) is summarized. The prospects for precision measurements of Higgs boson properties and Standard-Model processes as well as new physics scenarios beyond the Standard Model are given. Finally the concepts for an ultra-high-precision detector and R&D towards it are described.

*International Europhysics Conference on High Energy Physics*
*July 21st - 27th 2005*
*Lisboa, Portugal*

*Speaker.

© Copyright owned by the author(s) under the terms of the Creative Commons Attribution-NonCommercial-ShareAlike Licence. 

PoS(HEP2005)402

## 1. Challenges at the TeV-Scale and the ILC

Many of the most burning questions of microscopic physics will be addressed if we explore the TeV energy range, sometimes called the Terascale. The most prominent among these questions are:

1. What is the origin of electro-weak symmetry breaking? Is the Higgs mechanism at work or has Nature chosen a different solution?

2. Are there new symmetry laws which become visible at the Terascale? What is the origin of the large hierarchy between the electro-weak scale and the Planck scale? Are there hints towards a unification of all known forces?

3. What is the structure of our space-time? Are there compactified extra space dimensions, whose consequence become visible at the Terascale?

Furthermore, experimental particle physics at the Terascale becomes an increasingly important tool to answer questions of cosmology. In particular, the nature of dark matter and questions related to the Baryon asymmetry in the universe can be addressed if the Terascale is fully exploited.

With the start of the Large Hadron Collider LHC at CERN in 2007, it is very likely that an era of ground-breaking discoveries in the Terascale regime will start. The discoveries will set the scene for their further exploration and for the understanding of the underlying physics. It has been shown that the LHC can perform initial measurements of the properties of the new particles in many cases [1]. However a full exploration of Terascale physics will need additional experimental efforts. The complementarity of the possibilities at hadron and lepton colliders has already in the past proven to be essential for the understanding of high energy phenomena. Most notably the experimental verification of the Standard Model (SM) would not have been possible without the precise measurements of the LEP and SLC electron-positron colliders. Only the latter allowed for comprehensive tests of the coupling structure of the fundamental fermions and gauge bosons at the level of quantum corrections. To achieve this, precision at the percent-level is necessary which in many cases is only possible at lepton colliders. Our current view of particle physics which enables us to make solid predictions for Terascale physics and shapes the future experimental program for the LHC and beyond was only possible through the synergy created by hadron colliders and lepton colliders.

These measurements confirm the predictions of the SM in a very impressive way. Through quantum level analyses, it was possible to constrain the mass of the Higgs boson to below 200 GeV at the 95% confidence level within the SM and many of its possible extensions [2]. Furthermore many new physics scenarios acting at the Terascale could already be ruled out or at least severely constrained by these precision measurements.

The reason for the superior precision of measurements at electron-positron colliders is mainly due to the following reasons:

1. Point-like nature of the colliding particles which leads to a precise knowledge of the initial state;

2. Tunable collision energy, allowing for threshold scans;



PoS(HEP2005)402

3. Possibility to polarize both beams, allowing for detailed analysis of the helicity structure of the processes and sometimes significant suppression of backgrounds;
4. Moderate backgrounds from SM processes due to the only electro-weakly interacting initial state;
5. Moderate machine backgrounds.

In the past years, a broad world-wide consensus among particle physicists has emerged that a linear electron-positron collider operating at a centre-of-mass energy of up to 500 GeV in a first phase and upgradable to 1000 GeV be the next major collider facility for particle physics [3]. In 2004 the accelerator technology based on superconducting accelerating structures was selected for the world-wide project now called the International Linear Collider (ILC). For the ILC, the Global Design Effort (GDE) [4] has started in 2005 with the aim of arriving at a detailed technical design of the machine and the detectors in 2008/09. The baseline parameters for the machine are [5]

- electron-positron collisions at $M_Z \leq \sqrt{s} \leq 500$ GeV,
- electron and positron polarisation,
- integrated luminosity of at least 500 fb$^{-1}$ in the first four years,
- upgradability to about 1 TeV with 500 fb$^{-1}$ per year.

Further options for the machine include a high-luminosity running at $\sqrt{s} = M_Z$ (Giga-Z) and the possibility to provide $\gamma\gamma$ and $e\gamma$ collisions through Compton backscattering of an intense laser beam.

In the following I will discuss the expected capabilities of the ILC for the most important physics scenarios. Then I will discuss the challenges and status of the development for ILC detectors.

## 2. Physics Scenarios

The physics capabilities at the ILC are two-fold, *microscopic* and *telescopic*. The microscopic capability lies in the fact that any new particles which are kinematically accessible at ILC energies can be studied in great detail, i.e. its quantum numbers, decays, production modes, cross sections, and coupling structure. The telescopic capability relies on the fact that precise measurements of either SM or new particle differential cross sections can be used to look for quantum level effects arising from virtual particles in loops. This technique, already successfully exploited at LEP and SLC provides sensitivity to new particles and phenomena often deep into the multi-TeV region, far above the direct kinematical reach of the ILC.

In the past years, the physics case for the ILC has been studied in great detail and documented in numerous reports [6]. The general outcome of these studies is that independent of the what the LHC will (or will not) discover, the ILC has important and most often crucial measurements to perform. These will significantly enhance the understanding of the underlying physics. The precise tasks of the ILC of course depend on the LHC findings. A simple classification can be done in the following way:



PoS(HEP2005)402

1. If there is a light Higgs boson (consistent with precision electro-weak measurements): the ILC can verify that the Higgs mechanism is at work in all essential details.

2. If there is a heavy Higgs boson (inconsistent with precision electro-weak measurements): the ILC can again verify the Higgs mechanism in most details. In addition, precision measurements of SM processes will be important to find out why electro-weak radiative corrections are inconsistent with the observed Higgs mass.

3. Either light or heavy Higgs bosons and new particles in the kinematic reach of the ILC (e.g. supersymmetric particles, new states from extra dimension models, little Higgs models etc.): precise spectroscopy of the new states.

4. No Higgs boson at LHC, no new states: the ILC has to make sure that the LHC hasn't missed anything and perform precise measurements of SM processes in order to get a hint of multi-TeV phenomena responsible for EWSB and find out why precision data are inconsistent with SM radiative corrections.

In the following I will briefly describe the main measurements in the context of Higgs Bosons, Strong EWSB, Supersymmetry, and Top Quarks.

### 2.1 Higgs Boson Precision Physics

The anchor of a model-independent precision analysis of Higgs boson properties at a ILC is the measurement of the total cross-section for the Higgs-strahlung process, $e^+e^- \to H^0Z$. Z bosons can be selected in $Z \to e^+e^-$ and $Z \to \mu^+\mu^-$ decays [7]. From energy-momentum conservation, the invariant mass recoiling against the Z candidate can be calculated. Through a cut on the recoil mass, Higgs bosons can be selected independent of their decay mode, allowing for a model-independent measurement of the effective HZ coupling, $g_{HZZ}$. Once $g_{HZZ}$ is known, all other Higgs couplings can be determined *absolutely*. The total Higgs-strahlung cross-section can be measured with an accuracy of 2.5% for $m_H = 120$ GeV and $\sqrt{s} = 350$ GeV for 500 $fb^{-1}$ [8]. The corresponding recoil mass spectrum is shown in Fig. 1.

The measurements of differential production cross-sections and decay angular distributions provide access to the discrete quantum numbers of the Higgs boson: $J^{PC}$ [9]. The measurement of the $\beta$-dependence of the Higgs-strahlung cross-section close to the production threshold was exploited to determine the spin of the Higgs boson. The spin can also be determined from the invariant mass of the off-shell Z boson in the decay $H^0 \to ZZ^*$ for $m_H < 2m_Z$. For $m_H$ above $2m_Z$, azimuthal correlations of the two Z boson decay planes can be exploited to gain sensitivity to Higgs boson spin and CP [10].

The CP quantum number, like the spin, can be determined from both Higgs boson production and decay [11]. The angular distribution of the Z recoiling against the $H^0$ in Higgs-strahlung can be exploited. Furthermore, the transverse spin correlation in $H^0 \to \tau^+\tau^-$ decays can be used. The spin correlations between the two $\tau$ leptons is probed through angular correlations of their decay products.

The precise measurement of Higgs boson decay branching ratios is one of the key tasks in ILC Higgs physics. For a light Higgs boson with $m_H < 160$ GeV, a large variety of Higgs decay



PoS(HEP2005)402

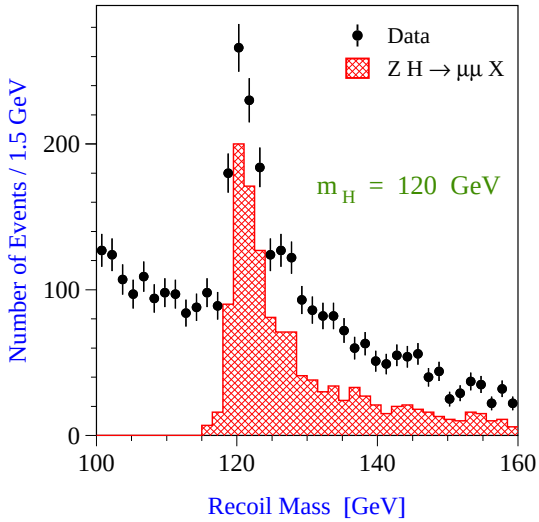


**Figure 1:** Recoil mass of events with two isolated muons consistent with a $Z^0$. The shaded histogram represents the contribution from $e^+e^- \to H^0Z^0$ events ($\sqrt{s} = 350$ GeV, 500 fb$^{-1}$, $m_H = 120$ GeV [8].

modes can be measured. The hadronic decays into $b\bar{b}, c\bar{c}$, and gg are disentangled via the excellent capabilities of an ILC vertex detector. Besides the decays into $b\bar{b}, c\bar{c}$, gg, $\tau^+\tau^-, W^+W^-$, $Z^0Z^0$, and $\gamma\gamma$ further decay modes have been studied. The very rare decay $H^0 \to \mu^+\mu^-$ is be detectable in WW-fusion events at $\sqrt{s} = 800$ GeV for $m_H = 120$ GeV. A measurement of the muon Yukawa coupling with approximately 15% relative accuracy may be obtained from a sample of 1 ab$^{-1}$.

For $m_H < 2m_t$, the top quark Yukawa coupling is not directly accessible from Higgs decays. The only relevant tree level process to access the top quark Yukawa coupling is the process $e^+e^- \to H^0t\bar{t}$ [12]. Due to the large masses of the final state particles, the process only has a significant cross-section at center-of-mass energies significantly beyond 500 GeV. For the $H^0 \to b\bar{b}$ decay, both the $t\bar{t} \to b\bar{b}q\bar{q}\ell^-\bar{\nu}$ and the $t\bar{t} \to b\bar{b}q\bar{q}q\bar{q}$ channels have been analyzed. For the $H^0 \to W^+W^-$ decay, the 2-like-sign lepton plus 6-jet and the single lepton plus 8-jet final states were studied. The expected uncertainties on the top Yukawa coupling for 1ab$^{-1}$ at 800 GeV range from 6–14% for $120 < m_H < 200$ GeV.

Invisibly decaying Higgs bosons are difficult to be detected at the LHC. In particular a measurement of the Higgs mass is almost impossible. At the ILC, there are two methods to measure the invisible Higgs branching ratio. The first proceeds through the comparison of the decay-mode-independent Higgs production rate with the total visible rate of Higgs decays. The second method explicitely requires a reconstructed Z-Boson accompanied by missing energy from the Higgs decay. At $\sqrt{s} = 350$ GeV, the achievable precision on the invisible branching ratio is $\sim 10\%$ for a branching ratio of 5% and a $5\sigma$ observation down to a branching ratio of 1.5-2.0% with 500 fb$^{-1}$ at $\sqrt{s} = 350$ GeV and Higgs masses between 120 and 160 GeV [13] can be achieved.

The observation of a non-zero self-coupling of the Higgs boson is the ultimate proof of spontaneous symmetry breaking being responsible for mass generation of the SM bosons and fermions since it probes the shape of the Higgs potential and thus the presence of a vacuum expectation value.



PoS(HEP2005)402

Higgs boson self-coupling in general leads to triple and quartic Higgs boson couplings out of which only the former are accessible. For 500 GeV center-of-mass energy, the double Higgs-strahlung process, $e^+e^- \to H^0H^0Z$ is most promising for observation, the small cross-section of 0.1 - 0.2 fb however demands the highest possible luminosity and calls for ultimate jet energy resolution since only if the most frequent six jet final state $b\bar{b}b\bar{b}q\bar{q}$ can be reconstructed, the signal rate becomes significant. The cross-section has been calculated in [14]. An experimental analysis for $m_H = 120$ GeV was presented [15] which concluded that with $1ab^{-1}$ of data at 500 GeV, a precision of 17 - 23 % for $120 < m_H < 140$ GeV on the $e^+e^- \to H^0H^0Z$ cross-section can be achieved. The potential of the WW-fusion channel for higher Higgs boson masses at higher energies was discussed and compared to the possibilities at the LHC in [16]. Further improvements can be obtained if kinematic differences between the signal diagram and diagrams which lead to the same final state without involving the triple Higgs coupling (dilution diagrams) are exploited [17].

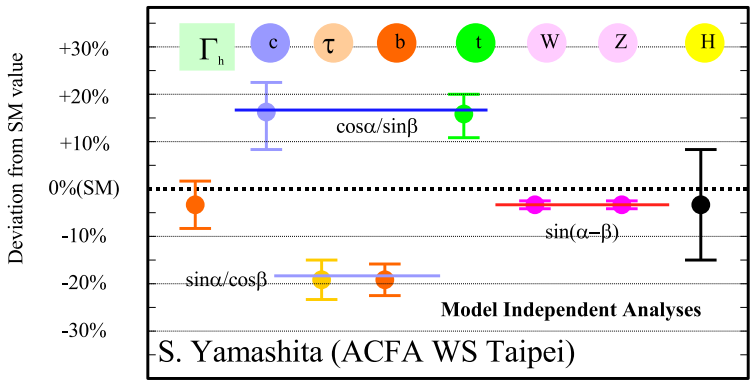


**Figure 2:** Deviation of the Higgs couplings in a two Higgs doublet model from the SM. The error bars denote the achievable precision at the ILC [18].

The achievable percent-level precision on Higgs boson couplings is sufficient to discriminate between different models. As shown in Fig. 2, distinct differences e.g. between a one-doublet model like the SM and two-doublet models can be exploited [18]. In Fig. 3, the ratio of the decay modes $h^0 \to b\bar{b}$ to $h^0 \to W^+W^-$ is shown relative to its SM value as a function of the mass of the heavy CP-odd Higgs mass $m_A$ for a broad scan of parameter points of the Minimal Supersymmetric Standard Model (MSSM) which are not otherwise distinguishable by LHC or ILC measurements. It can be seen $m_A$ can be significantly constrained up to masses of about 800 GeV [19].

### 2.2 No elementary Higgs boson

If no elementary Higgs boson exists, the scattering amplitude for longitudinally polarized weak gauge bosons, $W_LW_L \to W_LW_L$ violates unitarity at $\sqrt{s} \sim 1.2$ TeV unless new interactions set in. These new interactions may either involve a new strong interaction (Technicolor) or delay the unitarity violation by introduction new weakly couplings resonances, e.g. Kaluza-Klein excitations of gauge bosons(Higgsless models).

At the ILC these models can be analyzed in a model-independent way by the study of trilinear and quartic gauge boson couplings. Those can be parameterized by an effective Lagrangian [20]. In Fig. 4 (left), the sensitivity of the ILC to the coupling parameters $\alpha_4$ and $\alpha_5$ at $\sqrt{s} = 1$ TeV from



PoS(HEP2005)402

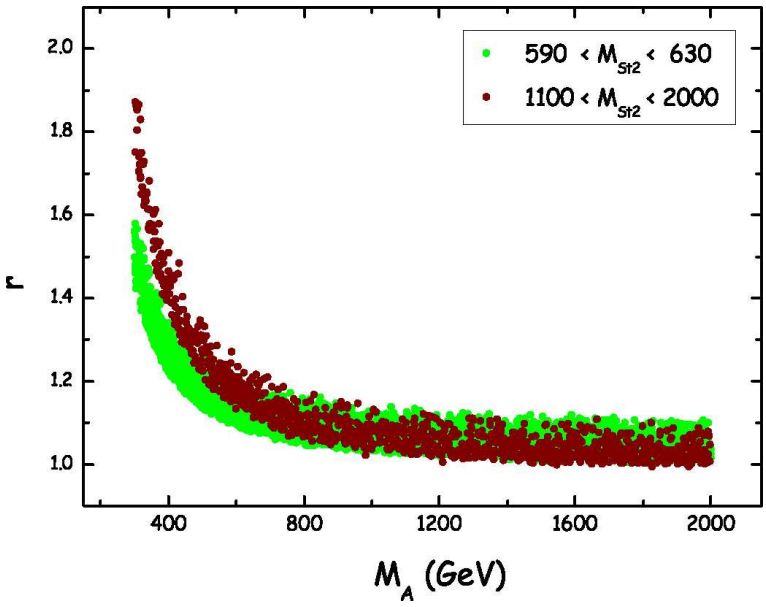


**Figure 3:** $BR(h \to b\bar{b})/BR(h \to WW)$ MSSM/SM within the as a function of $m_A$ for model points consistent with direct SUSY signals at LHC and ILC [19].

vector-boson scattering and three vector boson production are shown. The bounds correspond to mass limits of approximately 3 TeV for resonances with unit couplings [21].

If weakly coupled resonances can be produced kinematically at the ILC, they can naturally be studied in great detail. In Fig. 4(right) such a resonance, behaving like a sequential $Z'$ boson from a Higgsless model is shown [22]. Even if such resonances cannot be directly produced, their interference with the SM-$Z/\gamma$-propagator allows us to determine the vector-axial-vector coupling structure if the resonance mass is known e.g. from the LHC [23].

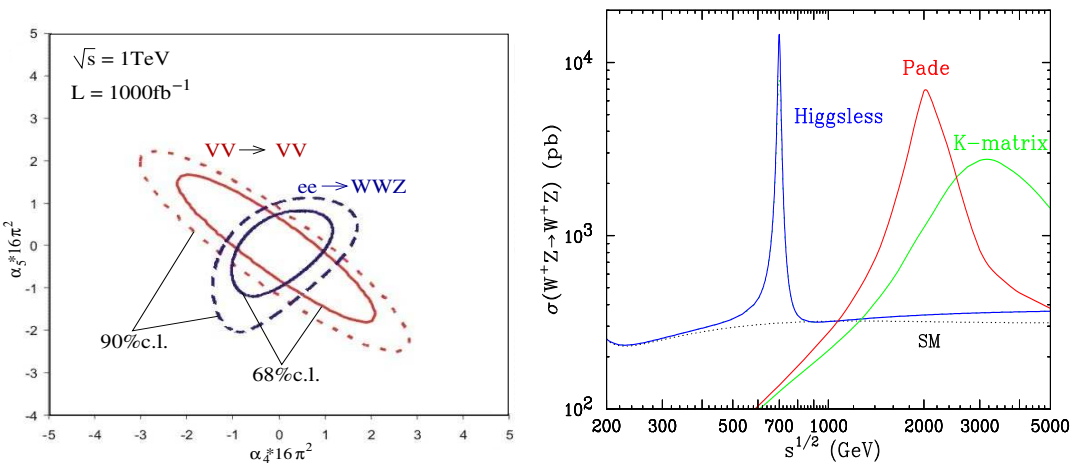


**Figure 4:** Left: constraints on quartic gauge couplings [21]. Right: Resonance in Higgsless model [22].



PoS(HEP2005)402

### 2.3 Supersymmetry

The search for Supersymmetry (SUSY) and, should it be found, measurements of the superpartner properties are among the most important motivations for future high energy particle colliders.

The LHC has a huge potential for SUSY discovery as well as for first measurements of SUSY particle properties. The ILC is an ideal tool for precision SUSY measurements. Both machines together will be able to give important insight into the mechanism of SUSY breaking and may open a window to GUT/Planck scale physics.

The precision SUSY analyses at the ILC greatly benefit from the possibility of tunable centre-of-mass energy and from the polarisablilty of both beams which allows for deciphering the coupling structure. For a large part of the SUSY parameter space, at least a large part of the color neutral sparticles are visible at the ILC in a variety of different production processes (see Fig. 5).

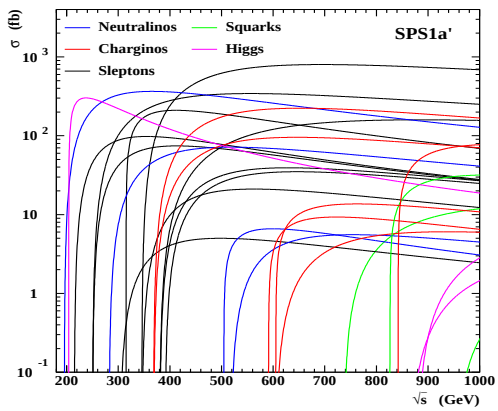


**Figure 5:** Left: SUSY production cross sections in $e^+e^-$ collisions for benchmark point SPS1a'. Right: Muon energy spectrum in smuon pair production [26].

The masses of the color-neutral superpartners can be measured in two different ways. First, in continuum production kinematic end-points of energy spectra can be used to extract simultaneously the involved masses. Second, the measurement of the shape of the production cross-section for various processes near threshold allows for a very precise extraction of the sum of the produced superpartner masses.

Sleptons are pair-produced in the reactions $e^+e^- \to \tilde{\ell}_i^+\tilde{\ell}_j^-$, $\tilde{\nu}_\ell\bar{\tilde{\nu}}_\ell$ via $s$-channel $\gamma/Z$ exchange and $t$-channel $\tilde{\chi}$ exchange for the first generation. As an example, in Fig. 6(left) the measurable energy spectrum of the muons from the process $e_L^+e_R^- \to \tilde{\mu}_R^+\tilde{\mu}_R^- \to \mu^+\tilde{\chi}_1^0\mu^-\chi_1^0$ is shown [24]. Events can be selected with negligible SM background. In particular background from W-pair production can be efficiently suppressed by choosing right-handed electrons in the initial state. SUSY backgrounds in this final state are generally small and can be suppressed by topological cuts. Due to the scalar nature of the smuons, the energy spectrum has a box shape. From the upper and lower end-points, the slepton and LSP masses can be determined.



PoS(HEP2005)402

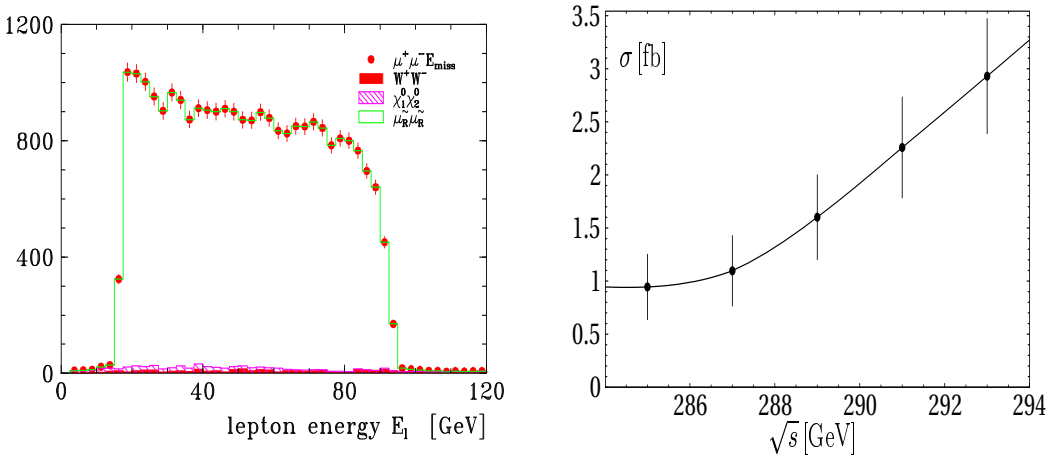


**Figure 6:** Left: Muon energy spectrum in smuon pair production [24]. Right:Threshold scan [25].

Alternatively, the slepton masses can be extracted from a threshold scan as shown in Fig. 6(right) for right selectron production both in $e^+e^-$ and $e^-e^-$ collisions and for right smuon production. With measurements at five center-of-mass energies with only 10 fb$^{-1}$ per point a precision of $\mathscr{O}$(100 MeV) can be achieved. With this precision higher-order corrections and final width corrections have to be taken into account [25].

Charginos and neutralinos are pair-produced $e^+e^- \to \tilde{\chi}_i^\pm \tilde{\chi}_j^\mp$ and $e^+e^- \to \tilde{\chi}_i^0 \tilde{\chi}_j^0$ via $s$-channel $\gamma/Z$ exchange and $t$-channel selectron or sneutrino exchange. The lightest chargino decays according to $\tilde{\chi}_1^\pm \to \ell^\pm \nu_\ell \tilde{\chi}_1^0$ either via an intermediate virtual or real $W^\pm$ boson or if kinematically possible via a real slepton. The second lightest neutralino decays according to $\tilde{\chi}_2^0 \to \ell^+\ell^- \tilde{\chi}_1^0$ either via a virtual or real $Z$ boson or via a real slepton. In particular, if $m_{\tilde{\nu}} < m_{\tilde{\chi}_2^0}$, invisible $\tilde{\nu}$ decays may occur. For large mixing in the stau sector and for large values of $\tan\beta$ the $\tilde{\tau}_1$ slepton is often much lighter than the other sleptons which can lead to a significant enhancement of $\tau$ leptons in the chargino and neutralino final states. The production processes for $\tilde{\tau}$, $\chi_2^0$ and $\chi_1^\pm$ may therefore all lead to the same $\tau^+\tau^-+$ missing energy signature. Topological cuts and the use of polarized beams can help to disentangle the contributing SUSY processes. As in the case of sleptons, the chargino and neutralino masses can be measured from the lepton energy and mass spectra as well as from threshold scans. In the more difficult case of exclusive decays into $\tau$ final states, a mass precision of a few GeV can be achieved in the continuum and 0.5 GeV from a threshold scan. Significantly better precision can be achieved if electron and muon final states are produced with sufficient rate [26].

Although squarks are often too heavy to be produced at a 1 TeV ILC, the light scalar top quark may be lighter than the other squarks and therefore accessible in the reaction $e^+e^- \to \tilde{t}_1\tilde{t}_1 \to b\tilde{\chi}_1^+ \bar{b}\tilde{\chi}_1^- \to b\tau^+\nu\tilde{\chi}_1^0 \bar{b}\tau^-\nu\tilde{\chi}_1^0$. The final state consists of two $b$-jets, two $\tau$'s and missing energy. The energy spectrum of the $b$-jets can be used to reconstruct the stop mass provided the neutralino and chargino masses are known. With a luminosity of 1000 fb$^{-1}$ the rate will be sufficient to achieve a mass resolution of 2 GeV. For a light scalar top quark, the decay chain $e^+e^- \to \tilde{t}_1\tilde{t}_1 \to\to c\tilde{\chi}_1^0 \bar{c}\tilde{\chi}_1^0$ has also been studied. From a measurement of the production cross-section with opposite



PoS(HEP2005)402

beam polarizations, a measurement of both mass and mixing angle can be inferred [27].

The achievable superpartner mass precision of the ILC for the SPS1a scenario is summarized in Table 1 taken from [28].

**Table 1:** Sparticle masses and their expected precisions in Linear Collider experiments, SPS 1a mSUGRA scenario (from [28]).

| | $m$ [GeV] | $\Delta m$ [GeV] | Comments |
|---|---|---|---|
| $\tilde{\chi}_1^\pm$ | 176.4 | 0.55 | simulation threshold scan , 100 fb$^{-1}$ |
| $\tilde{\chi}_2^\pm$ | 378.2 | 3 | estimate $\tilde{\chi}_1^\pm\tilde{\chi}_2^\mp$, spectra $\tilde{\chi}_2^\pm \to Z\tilde{\chi}_1^\pm, W\tilde{\chi}_1^0$ |
| $\tilde{\chi}_1^0$ | 96.1 | 0.05 | combination of all methods |
| $\tilde{\chi}_2^0$ | 176.8 | 1.2 | simulation threshold scan $\tilde{\chi}_2^0\tilde{\chi}_2^0$, 100 fb$^{-1}$ |
| $\tilde{\chi}_3^0$ | 358.8 | 3 – 5 | spectra $\tilde{\chi}_3^0 \to Z\tilde{\chi}_{1,2}^0$, $\tilde{\chi}_2^0\tilde{\chi}_3^0, \tilde{\chi}_3^0\tilde{\chi}_4^0$, 750 GeV, $>$ 1000 fb$^{-1}$ |
| $\tilde{\chi}_4^0$ | 377.8 | 3 – 5 | spectra $\tilde{\chi}_4^0 \to W\tilde{\chi}_1^\pm$, $\tilde{\chi}_2^0\tilde{\chi}_4^0, \tilde{\chi}_3^0\tilde{\chi}_4^0$, 750 GeV, $>$ 1000 fb$^{-1}$ |
| $\tilde{e}_R$ | 143.0 | 0.05 | $e^-e^-$ threshold scan, 10 fb$^{-1}$ |
| $\tilde{e}_L$ | 202.1 | 0.2 | $e^-e^-$ threshold scan 20 fb$^{-1}$ |
| $\tilde{\nu}_e$ | 186.0 | 1.2 | simulation energy spectrum, 500 GeV, 500 fb$^{-1}$ |
| $\tilde{\mu}_R$ | 143.0 | 0.2 | simulation energy spectrum, 400 GeV, 200 fb$^{-1}$ |
| $\tilde{\mu}_L$ | 202.1 | 0.5 | estimate threshold scan, 100 fb$^{-1}$ |
| $\tilde{\tau}_1$ | 133.2 | 0.3 | simulation energy spectra, 400 GeV, 200 fb$^{-1}$ |
| $\tilde{\tau}_2$ | 206.1 | 1.1 | estimate threshold scan, 60 fb$^{-1}$ |
| $\tilde{t}_1$ | 379.1 | 2 | estimate $b$-jet spectrum, $m_{\min}(\tilde{t})$, 1TeV, 1000 fb$^{-1}$ |

Besides the precise measurement of the largest possible set of superpartner masses the measurement of quantum numbers, couplings, and mixings plays an important role in deciphering the supersymmetric model. In $e^+e^-$ collisions, due to the low background and the known initial state, various possibilities to extract quantum numbers and couplings exist. These range from the measurement of inclusive rates to the measurement of angular distributions in production and decay.

The fundaments of SUSY rely on the superpartners' spin differing by $\frac{1}{2}$ from their SM partners. At the ILC, the spins of the superpartners can be determined directly from the production angle distributions. The scalar leptons exhibit a $\sin^2\theta$ distribution which can be reconstructed up to a twofold ambiguity in smuon pair-production. The situation is more complicated for charginos and neutralinos which exhibit a forward-backward asymmetry in the production angle due to their mixed U(1) and SU(2) couplings and the additional t-channel contribution. The forward-backward asymmetry and in particular the left-right polarization asymmetry provide sensitive observables in order to disentangle the chargino and neutralino mixing matrices [29].

In SUSY, the chiral (anti-)fermions are associated in an unambiguous way to scalars, i.e. $e^-_{L,R} \leftrightarrow \tilde{e}^-_{L,R}$ and $e^+_{L,R} \leftrightarrow \tilde{e}^+_{R,L}$. The four pair-production processes for left and right selectrons, $e^+e^- \to \tilde{e}^+_R\tilde{e}^-_R$, $e^+e^- \to \tilde{e}^+_L\tilde{e}^-_L$, $e^+e^- \to \tilde{e}^+_R\tilde{e}^-_L$, $e^+e^- \to \tilde{e}^+_L\tilde{e}^-_R$ can be disentangled from their different dependence of the cross-section to polarized electron and positron beams [30]. The t-channel contribution to the production cross-sections is sensitive to the SUSY Yukawa coupling $\hat{g}(e\tilde{e}\tilde{\chi}^0)$ which is fundamentally related to the SM gauge couplings. The SU(2) and U(1) SUSY Yukawa couplings can be determined to a precision of 0.7% and 0.2%, respectively with 500 fb$^{-1}$ at 500 GeV in a SPS1a scenario [24].



PoS(HEP2005)402

The ultimate goal of measurements of the properties of superpartners at LHC and ILC will be the extraction of the complete set of parameters of the low energy MSSM Lagrangian. At tree level, the parameter determination can proceed sector by sector, e.g. the chargino sector is completely determined by the three parameters $M_2, \mu, \tan\beta$. However, with the anticipated precision of ILC measurements, higher order corrections to masses, cross-sections, and branching ratios are not negligible. At loop-level in principle every observable depends on the full set of SUSY parameters. An analytic procedure to extract the Lagrangian parameters from data is no longer possible. Instead, a global fit of the Lagrangian parameters to the complete set of SUSY observables at LHC and ILC will be necessary.

Two programs, SFITTER [31] and Fittino [32] have been developed to achieve this goal. As an example, a recent result from Fittino is explained here. A MSSM with 19 free parameters has been chosen as the theoretical basis. It is derived from the full MSSM but assuming real couplings, flavour diagonal sfermion mass matrices and universality of the soft SUSY breaking parameters of the first two generations. For the theoretical predictions for the observables as a function of the parameters the SPHENO [33] program has been used which includes higher-order corrections wherever they have been calculated. It should be noted that neither LHC nor ILC input alone can constrain the assumed model enough to yield a converging fit. The definition of a scheme to extract well-defined parameters at higher orders is currently being worked out in the Supersymmetry Parameter Analysis (SPA) project [34].

The extracted parameters of the electro-weak scale MSSM Lagrangian can then be extrapolated to high (GUT, Planck) scales (Fig. 8 in order to determine distinct patterns of unification and reconstruct the underlying fundamental theory of SUSY breaking [35].

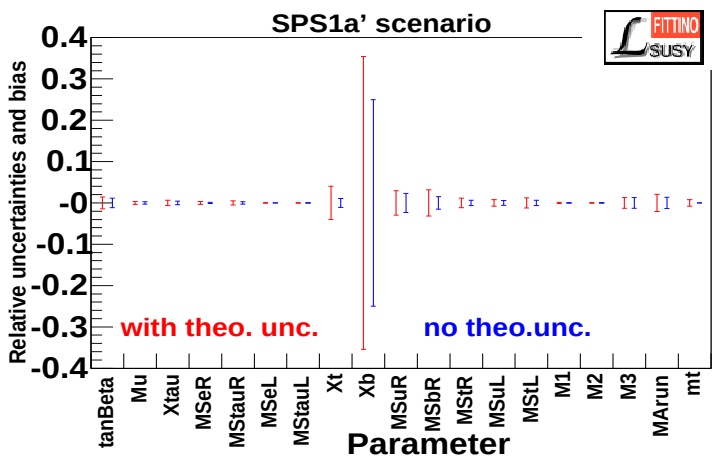


**Figure 7:** Relative uncertainties of SUSY parameters obtained from a global fit to LHC and ILC observables [32].

### 2.4 Connection to Cosmology: The Nature of Dark Matter

The SUSY LSP provides an excellent candidate for dark matter. Measurements of temperature fluctuations of the cosmic microwave background by the WMAP satellite [36] strongly constrain the SUSY LSP properties and therefore point to certain regions in the MSSM parameter space.



PoS(HEP2005)402

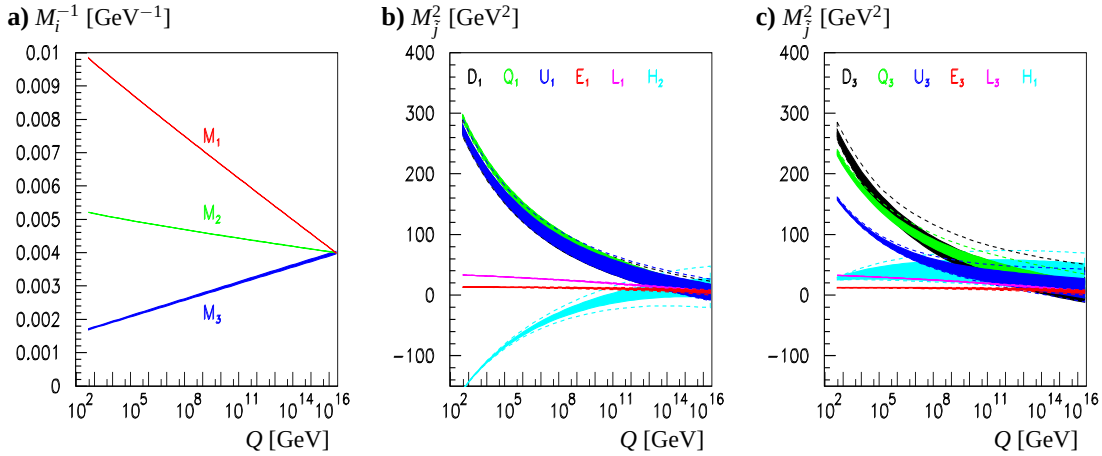


**Figure 8:** Running of **a)** the gaugino mass parameters, **b)** first generation scalar mass parameters and $M_{H_2}^2$ and **c)** third generation scalar mass parameters and $M_{H_1}^2$ in SPS1a′. Full bands: only experimental errors are taken into account; dashed lines: today's theoretical errors are taken into account as a conservative estimate [32].

Of particular interest for experimental studies at colliders is the co-annihilation region in which the neutralino annihilation is enhanced by the t-channel process $\tilde{\chi}\tilde{\tau} \to \tau\gamma$ which contributes significantly only if the mass difference $\Delta m = m(\tilde{\tau}) - m(\tilde{\chi}_1^0)$ is small. The relic dark matter density depends critically on this mass difference. With the next generation of CMB experiments, in particular Planck, the DM density can be measured at the 2-3% level. It is therefore imperative to match this precision at colliders.

If $\Delta m$ is small (typically below 10 GeV), the staus decay with small visible energy and the signature is only a few soft charged tracks accompanied by large missing energy. Two-photon background is becoming severe unless it can be efficiently vetoed by the detection of very forward scattered electrons. In the very forward region significant energy induced by beam-beam-interactions is deposited.

The pair production of staus in the small-$\Delta m$ region has been studied in [37, 38, 39] for various MSSM parameter sets. With appropriate cuts, detection and a precise measurement of the $\tilde{\tau}$ mass is possible down to $\Delta m \sim$3 GeV. The resulting precision on the prediction for the dark matter density ranges from 2 to 6%, depending on the $\tilde{\tau}$ mass and on $\Delta m$. This precision matches the anticipated precision of the Planck satellite of 2%. As an example the hadronic energy spectra for $\tau$ decays from the process $e_L^+ e_R^- \to \tilde{\tau}_1 \tilde{\tau}_1 \to \tau^+ \tilde{\chi}_1^0 \, \tau^- \tilde{\chi}_1^0$ as shown after detector simulation and cuts together with the two-photon background for $\Delta m = 5$ GeV (Model Point D′ from [40]).

### 2.5 Precision Measurement of the Top Quark Mass

At the ILC, the mass of the heaviest quark, the top quark, can be measured very precisely from a scan of the production threshold for the process $e^+e^- \to t\bar{t}$. The statistical accuracy of the top mass and decay width is possible to 34 and 42 MeV, respectively, from a scan with 100 fb$^{-1}$ of data [41]. The largest uncertainty comes from the theoretical control of the cross section. With an appropriate mass definition and next-to-next-to-leading logarithm (NNLL) calculation being available, an extraction of $m_t$ with $\sim$ 100 MeV precision will be possible (Fig. 9 (left)) [42].



PoS(HEP2005)402

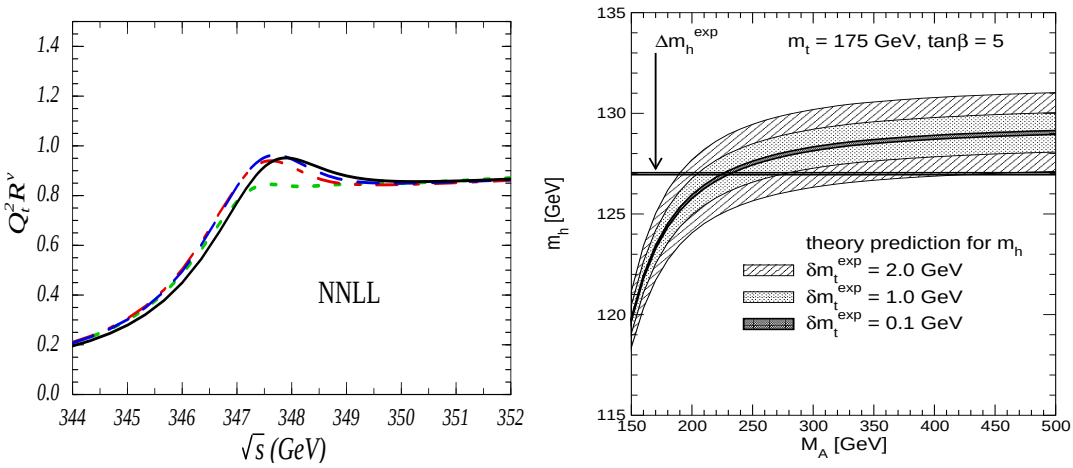


**Figure 9:** Left: NNLO calculation of $e^+e^- \rightarrow$ cross section close to production threshold for different values of the top velocity parameter [42]. Right: Allowed region for $m_h$ as a function of $m_A$ for different uncertainties of $m_t$ [43].

A precise knowledge of the top quark mass is desirable a such, since it is a fundamental SM parameter. Furthermore, when $m_H$ will be measured to 50 MeV precision, the top mass will be the precision limiting number in many theoretical predictions of beyond-SM physics. As an example the strong impact of $m_t$ on the prediction of the light Higgs boson mass as a function of $m_A$ in the MSSM is shown in Fig. 9(right) [43].

## 3. Detector Design for the ILC

The enormous statistical power of the ILC machine and the favourable background conditions should be matched by a precision detector which is capable of taking collision data with the least possible introduction of biases and systematic errors. Given the relatively low interaction rates, it will be possible to construct a data acquisition system without any hardware trigger allowing for event filtering after full reconstruction of the events. The required resolutions to achieve the statistically possible resolution are challenging for most of the subsystems. In particular the reconstruction of hadronic final states requires an unprecedented jet energy resolution. In order to achieve this goal, the particle flow concept has been chosen by most studied detector designs. This concept will be explained in the next section. Then the different detector designs which are currently developed in international detector concept studies are briefly described. Finally a short overview about ongoing sub-system R&D for vertex detectors, charged particle tracking and calorimetry is given.

### 3.1 The Particle Flow Concept

The particle flow concept is guided by the idea that the optimal jet energy resolution is achieved if all particles originating from the primary $e^+e^-$-collision are fully reconstructed individually. If this can be achieved, the best possible method to reconstruct the energy or the momentum of each particle species can be chosen depending on the nature of the particle. In particular, charged particle momenta can be measured from the tracking system with a resolution typically far superior



PoS(HEP2005)402

to the calorimetric measurement for the momenta relevant at ILC collisions. Electromagnetically interacting particles can be measured in the electro-magnetic calorimeter and only the energy measurement for the remaining roughly 10% of neutral hadrons has to rely on the hadronic calorimeter which typically has the worst individual energy resolution. Clearly the goal of ideal particle separation can only be reached approximately since electromagnetic and hadronic showers of all particles will overlap in the calorimeter. In order to realize the particle flow concept efficiently, the showers of individual particles must be made visible inside the calorimeter. This requires a fine segmentation of the calorimeters in three dimensions. Furthermore, a large magnetic field and/or a large inner radius of the calorimeter helps to disentangle charged and neutral particles in dense jets.

The importance of good jet energy resolution is illustrated in Fig. 10. Here the reconstructed mass of two hadronically decaying weak gauge bosons (WW or ZZ) in the process $e^+e^- \rightarrow \nu\bar{\nu}WW/ZZ$ are shown for 60% (left) and 30% (right) are shown. A jet energy resolution of 60% was reached in the ALEPH experiment. Clearly this would not be sufficient to disentangle the two processes in a satisfactory way. In order to arrive at 30%, which is the goal for the ILC detectors, a radically new calorimeter approach has to be followed.

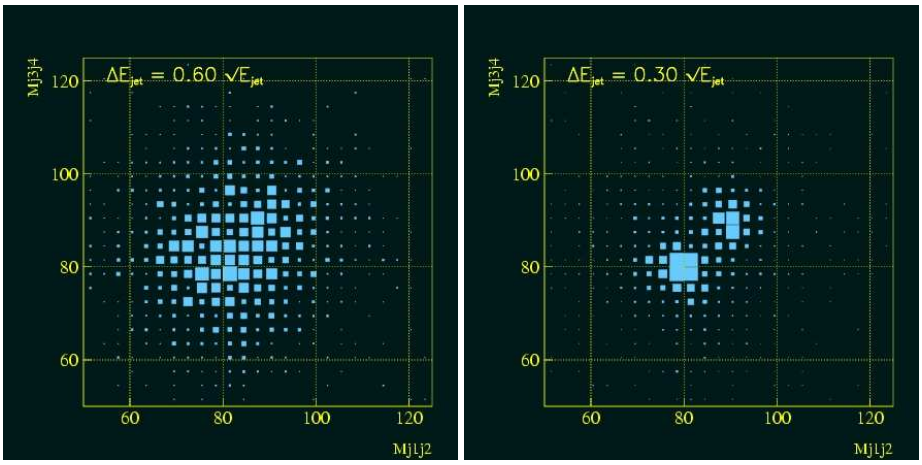


**Figure 10:** Reconstructed masses of hadronically decaying W- and Z-boson pairs in the process $e^+e^- \rightarrow \nu\bar{\nu}WW/ZZ$ for a jet energy resolution of 60% (left) and 30% (right).

Currently three overall detector concepts are studied. All are pursuing the particle flow concept. The main differences are in the choices for charged particle tracking and in the magnetic field and inner radius of the electromagnetic calorimeter. The *SiD* concept [44] employs a 5 T magnetic field and an all-silicon tracking system. The *LDC* concept [45] has a 4 T field and relies on a large time projection chamber (TPC) supplemented by few layers of silicon detectors for tracking. In the *GLD* concept [46] a 3 T magnetic field is compensated by an even larger calorimeter radius. While both in *SiD* and *LDC* a Silicon-Tungsten electromagnetic calorimeter(ECAL) with 1 $cm^2$ cells is foreseen, *GLD* relies on a Scintillator-Tungsten ECAL with crossed $1\times4$ $cm^2$ Sc-Tiles. The inner radius of the ECAL is 125/168/186 cm for SiD/LDC/GLD.

R&D on the crucial detector components has started in a world-wide effort. In most cases the R&D on the sub-detectors is independent of the specific detector design concept in which it would be implemented. Recently, a EU-funded program to improve the infrastructure for ILC detector



PoS(HEP2005)402

R&D, EUDET, has been approved [47]. An world-wide register of detector R&D for the ILC is kept at [48].

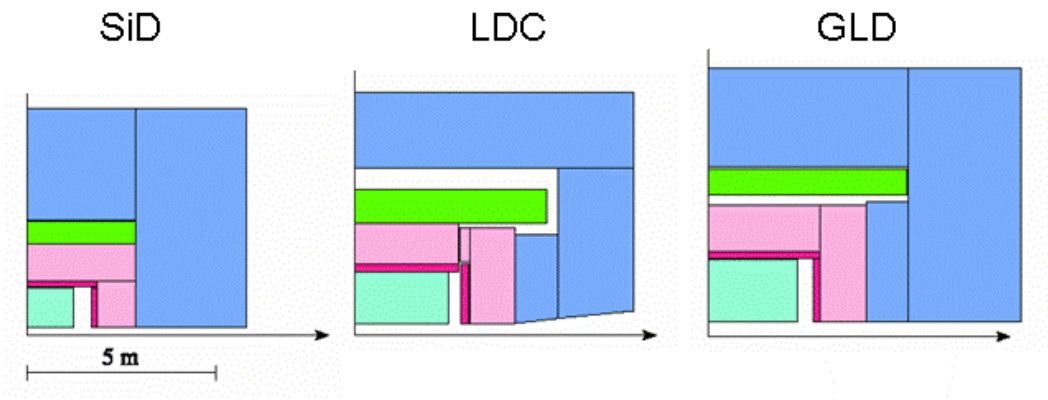


**Figure 11:** Three detector concepts

### 3.2 Vertex Detectors

High precision vertex detectors are mandatory at the ILC for the tagging of bottom and charm hadron as well as measuring the impact parameters of tau lepton decays products. Driving physics questions are the measurement of the Higgs branching ratios, in particular the separation of $H \to b\bar{b}$ and $H \to c\bar{c}$. Due to the extremely small beam-spot and the possibility of a beam-pipe radius as low as 1 cm, unprecedented flavour tagging will be possible. There is a general consensus that a four to five layered fine-grained ($<20\times20\mu m^2$) silicon pixel detector will be used. The challenge lies in the minimization of the necessary material to limit multiple scattering and secondary interactions as well as achieving the necessary readout speed. Various technologies are under active study: CCDs [49], DEPFET pixels [50], CMOS pixel sensors [51] and others.

### 3.3 Charged Particle Tracking

In the context of the particle flow concept, the requirements for charged particle tracking are mainly high efficiency, robustness, and good double track resolution. Here momentum resolution is less important. However for some important physics channels very high momentum resolution is mandatory. The most prominent example is the model-independent reconstruction and mass measurement of the Higgs boson exploiting the recoil mass technique. Here, the goal is to reconstruct the mass of the $Z \to \ell\ell$ decays to precision much better than the natural width of the $Z$-boson. In order to achieve this, a momentum resolution $\sigma(1/p_t) = 5 \times 10^{-5}\mathrm{GeV}^{-1}$ has to be achieved, approximately a factor five better than achieved at LEP.

Two complementary approaches to achieve this are pursued: Silicon strip detectors which give a small ($\sim 5$) number of very precise (few $\mu$m) space points or a huge Time Projection Chamber with at least 200 space points of moderate ($< 100\mu$m) point resolution.

In the case of Silicon tracking the major challenges are to achieve the desired point resolution with a minimum of material to reduce multiple scattering and photon conversions. Sensor R&D



PoS(HEP2005)402

and development of new readout ASIC's in deep-sub-micron technology has started within the international SiLC collaboration [52].

R&D for a large high precision TPC is ongoing in the international LC-TPC collaboration [53]. The main topics are the construction of low-material-budget field cage, the development of new gas amplification end-plates using micro-pattern gas-detectors like Micromegas and GEMs. Numerous small prototypes have already been tested in test beams at DESY and KEK inside large magnetic fields. The upcoming major goal is the construction of a large prototype (diameter $\sim$ 80 cm), which can be used to test all major design issues of the system.

### 3.4 Calorimetry

The challenge to construct a particle flow calorimeter is taken up by the world-wide CALICE collaboration [54]. The goal is to construct a fine-grained electro-magnetic and hadronic sampling calorimeter optimized for particle flow analysis. The calorimeter has to be very compact in order to fit inside the solenoid. For the ECAL currently 40 layers of Tungsten interleaved by 1x1 $cm^2$ segmented Silicon detectors as active layers is planned. For the HCAL either stainless steel or Tungsten as absorber are under consideration. The active layer may either consist of scintillator tiles with Silicon photomultiplier readout with analogue readout (size 5x5 $sm^2$) or digital readout with even higher granularity of 1x1 $cm^2$. The construction of such a fine-grained calorimeter needs a significant improvement in the understanding of the details of hadronic showers. The construction of a 1 $m^3$ prototype is underway and a beam test is the midterm goal of the project.

## 4. Conclusions

Supported by a broad consensus, the ILC should be the next major enterprise in accelerator based particle physics. It offers tremendous physics capabilities highly complementary to that of the LHC. LHC and ILC together allow for a comprehensive study of Terascale physics and are powerful tools to enhance our knowledge about microscopic physics in the coming decades. With the consensus about the choice of accelerating technology and the GDE process having started, the ILC design is put on a firm basis. As a part of this process, the development of a high-resolution ILC detector has started in a world-wide collaborative effort.

## 5. Acknowledgements

The author would like to thank the organizers of the HEP2005 conference in Lisboa for their hospitality and excellent organization of the sessions. The results presented in this talk are the work of many colleagues whose work is greatly acknowledged. In particular K. Mönig helped in the preparation of the talk and P. Wienemann helped in the preparation of these proceedings.

## References

[1] J. G. Branson, D. Denegri, I. Hinchliffe, F. Gianotti, F. E. Paige and P. Sphicas [ATLAS and CMS Collaborations], Eur. Phys. J. directC **4** (2002) N1.

[2] LEP Electro-Weak Working Group, hep-ex/0511027.



PoS(HEP2005)402

[3] http://www-flc.desy.de/lcsurvey/

[4] http://www.fnal.gov/directorate/icfa/ILC_GDE_MOU.pdf

[5] http://www.fnal.gov/directorate/icfa/LC_parameters.pdf

[6] H. Murayama and M. E. Peskin, Ann. Rev. Nucl. Part. Sci. **46** (1996) 533, hep-ex/9606003;
E. Accomando *et al.* [ECFA/DESY LC Physics Working Group], Phys. Rept. **299** (1998) 1, hep-ph/9705442;
J. A. Aguilar-Saavedra *et al.*, *TESLA Technical Design Report Part III: Physics at an $e^+e^-$ Linear Collider*, DESY-01-011C;
T. Abe *et al.* [American Linear Collider Working Group], "Linear collider physics resource book for Snowmass 2001", hep-ex/0106055 (part 1), hep-ex/0106056 (part 2), hep-ex/0106057 (part 3), and hep-ex/0106058 (2001), SLAC-R-570;
K. Abe *et al.* [ACFA Linear Collider Working Group Collaboration], hep-ph/0109166.

[7] J. R. Ellis, M. K. Gaillard and D. V. Nanopoulos, Nucl. Phys. B **106** (1976) 292; B. L. Ioffe and V. A. Khoze, Sov. J. Part. Nucl. **9** (1978) 50; B. W. Lee, C. Quigg and H. B. Thacker, Phys. Rev. Lett. **38** (1977) 883.

[8] P. Garcia-Abia and W. Lohmann, Eur. Phys. J. directC **2** (2000) 2.

[9] S. Y. Choi, D. J. Miller, M. M. Mühlleitner and P. M. Zerwas, *Identifying the Higgs Spin and Parity in Decays to Z Pairs*, Phys. Lett. B **553** (2003) 61, hep-ph/0210077, LC-TH-2003-036 (2003);

[10] V. D. Barger, K. m. Cheung, A. Djouadi, B. A. Kniehl and P. M. Zerwas, Phys. Rev. D **49** (1994) 79, hep-ph/9306270.

[11] M. Kramer, J. H. Kühn, M. L. Stong, and P. M. Zerwas, Z. Phys. **C64** (1994) 21, hep-ph/9404280;
B. Grządkowski and J. F. Gunion, Phys. Lett. **B350** (1995) 218, hep-ph/9501339;
K. Desch, Z. Was and M. Worek, *Measuring the Higgs boson parity at a linear collider using the tau impact parameter and tau → rho nu decay,*Eur. Phys. J. C **29** (2003) 491, hep-ph/0302046, LC-PHSM-2003-003 (2003).

[12] A. Djouadi, J. Kalinowski and P. M. Zerwas, Mod. Phys. Lett. A **7** (1992) 1765;
Y. You, W. G. Ma, H. Chen, R. Y. Zhang, S. Yan-Bin and H. S. Hou, Phys. Lett. B **571** (2003) 85, hep-ph/0306036;
G. Belanger *et al.*, Phys. Lett. B **571** (2003) 163, hep-ph/0307029;
A. Denner, S. Dittmaier, M. Roth and M. M. Weber, hep-ph/0307193.

[13] M. Schumacher, *Investigations of invisible decays of the Higgs boson at a futire e+e- linear collider,*LC-PHSM-2003-096.

[14] A. Djouadi, W. Kilian, M. Mühlleitner and P. M. Zerwas, Eur. Phys. J. C **10** (1999) 27, hep-ph/9903229;
Z. Ren-You, M. Wen-Gan, C. Hui, S. Yan-Bin and H. Hong-Sheng, hep-ph/0308203;
G. Belanger *et al.*, Phys. Lett. B **576** (2003) 152, hep-ph/0309010.

[15] C. Castanier, P. Gay, P. Lutz and J. Orloff, *Higgs self coupling measurement in e+ e- collisions at center-of-mass energy of 500 GeV* , LC-PHSM-2000-061 (2000).

[16] U. Baur, T. Plehn and D. Rainwater, *Examining the Higgs boson potential at lepton and hadron colliders: A comparative analysis*, hep-ph/0304015.

[17] M. Battaglia, E. Boos and W. M. Yao, in *Proc. of the APS/DPF/DPB Summer Study on the Future of Particle Physics (Snowmass 2001)* ed. N. Graf, eConf **C010630** (2001) E3016, hep-ph/0111276.



PoS(HEP2005)402

[18] S.Yamashita talk presented at the 7th ACFA workshop, Taipei, November 2004.

[19] K. Desch, E. Gross, S. Heinemeyer, G. Weiglein and L. Zivkovic, JHEP **0409** (2004) 062, hep-ph/0406322.

[20] W. Kilian and J. Reuter, hep-ph/0507099.

[21] P. Krstonosic *et al.*, hep-ph/0508179.

[22] A. Birkedal, K. Matchev and M. Perelstein, Phys. Rev. Lett. **94** (2005) 191803 [hep-ph/0412278];; A. Birkedal, K. T. Matchev and M. Perelstein, hep-ph/0508185.

[23] S. Riemann, PREL-LCPHSM-2003-24; S. Riemann, LC-TH-2001-007.

[24] A. Freitas, H. U. Martyn, U. Nauenberg and P. M. Zerwas, hep-ph/0409129; H. U. Martyn, hep-ph/0406123.

[25] A. Freitas, A. von Manteuffel and P. M. Zerwas, Eur. Phys. J. C **34** (2004) 487, hep-ph/0310182.

[26] Y. Kato et al, APPI Winter Institute, February 2003; K. Desch, talk at ECFA/DESY LC workshop Prague, November 2002, http://www-hep2.fzu.cz/ecfadesy/Talks/SUSY/; B. Sobloher, PhD Thesis in preparation; U. Nauenberg, talk at ECFA/DESY LC workshop Prague, November 2002, http://www-hep2.fzu.cz/ecfadesy/Talks/SUSY/.

[27] A. Finch, H. Nowak, A. Sopczak, "Scalar Top Mass Measurements at a Future LC", in proceedings of LCWS, Paris, 2004.

[28] G. Weiglein *et al.* hep-ph/0410364.

[29] G. Moortgat-Pick, A. Bartl, H. Fraas and W. Majerotto, Eur. Phys. J. C **18** (2000) 379, hep-ph/0007222.

[30] G. Moortgat-Pick, hep-ph/0410118; G. Moortgat-Pick *et al.*, hep-ph/0507011.

[31] R. Lafaye, T. Plehn and D. Zerwas, hep-ph/0404282.

[32] P. Bechtle, K. Desch and P. Wienemann, Comput. Phys. Commun. **174** (2006) 47, hep-ph/0412012; P. Bechtle, K. Desch, W. Porod and P. Wienemann, hep-ph/0511006, accpeted by Eur. Phys. J. C.

[33] W. Porod, Comput. Phys. Commun. **153** (2003) 275, hep-ph/0301101.

[34] J. A. Aguilar-Saavedra *et al.*, arXiv:hep-ph/0511344.

[35] G. A. Blair, W. Porod and P. M. Zerwas, Eur. Phys. J. C **27** (2003) 263 [hep-ph/0210058]; B. C. Allanach, G. A. Blair, S. Kraml, H. U. Martyn, G. Polesello, W. Porod and P. M. Zerwas, hep-ph/0403133.

[36] D. N. Spergel *et al.* [WMAP Collaboration], Astrophys. J. Suppl. **148** (2003) 175, astro-ph/0302209.

[37] H. U. Martyn, hep-ph/0408226.

[38] P. Bambade, M. Berggren, F. Richard and Z. Zhang, hep-ph/0406010.

[39] J. L. Feng, hep-ph/0509309.

PoS(HEP2005)402

[40] M. Battaglia, A. De Roeck, J. R. Ellis, F. Gianotti, K. A. Olive and L. Pape, Eur. Phys. J. C **33** (2004) 273 [hep-ph/0306219].

[41] M. Martinez and R. Miquel, Eur. Phys. J. C **27** (2003) 49, hep-ph/0207315.

[42] A. H. Hoang *et al.*, Phys. Rev. D **65** (2002) 014014, hep-ph/0107144.

[43] S. Heinemeyer, S. Kraml, W. Porod and G. Weiglein, JHEP **0309** (2003) 075, hep-ph/0306181.

[44] SiD concept, http://www-sid.slac.stanford.edu

[45] LDC concept, http://www.ilcldc.org

[46] GLD concept, http://ilcphys.kek.jp/gld

[47] http://www.eudet.org

[48] http://wiki.lepp.cornell.edu/wws

[49] LCFI Collaboration, http://hepwww.rl.ac.uk/lcfi/

[50] R. Kohrs *et al.*, IEEE Trans. Nucl. Sci. **52** (2005) 1171.

[51] G. Deptuch *et al.*, Nucl. Instrum. Meth. A **535** (2004) 366; http://ireswww.in2p3.fr/ires/recherche/capteurs/

[52] SILC Collaboration, http://silc.in2p2.fr

[53] LC-TPC R&D Collaboration, https://wiki.lepp.cornell.edu/wws/bin/view/Projects/TrackLCTPCcollab

[54] CALICE Collaboration, http://polywww.in2p3.fr/flc/calice.html

PoS(HEP2005)402